A face-based smoothed XFEM for three-dimensional fracture problems

[*]Y. Jiang[1], T.E. Tay[2], and Eric Li[3]

[1]Department of Engineering Mechanics, Institute of High Performance Computing, 1 Fusionopolis Way, Connix, Singapore 138632

[2]Department of Mechanical Engineering, National University of Singapore, 9 Engineering Drive 1, Singapore 117576

[3]School of Aerospace, Mechanical and Mechatronic Engineering, The University of Sydney, Sydney, NSW 2006, Australia

∗ Corresponding author: jiangyo@ihpc.a-star.edu.sg

Abstract

In this work, a face-based smoothed extended finite element method (FS-XFEM) is developed for three-dimensional fracture problems. This method combines the extended finite element method (XFEM) and smoothing technique together. With XFEM, arbitrary crack geometry can be modeled and crack advance can be simulated without remeshing. With face-based smoothing technique, the integration of singular term over the volume around the crack front can be eliminated, thanks to the transformation of volume integration into area integration. Numerical examples are presented to test the accuracy and convergence rate of the FS-XFEM. From the results, it is clear smoothing technique can improve the performance of XFEM for three-dimensional fracture problems

Keywords: three-dimension, face-based smoothed extended finite element method, stress intensity factor.

1. Introduction

The fracture analysis by standard finite element method (FEM) is quite cumbersome and tedious caused by conforming the crack geometry to element boundary. Remeshing, which greatly increases the computation time, is always needed to match the new geometry of the crack surface, when the crack advances. In order to avoid these two disadvantages of FEM, the extended finite element method (XFEM) has been proposed to facilitate the modeling of arbitrary crack geometry and its evolvement [Belytschko et al. (1999); Moes et al. (1999);]. In the XFEM, the displacement field of the standard FEM is enriched by a discontinuous displacement function and the asymptotic displacement field around the crack tip based on a local partition of unity. The most important advantage of XFEM is that it can simulate the crack without conforming the mesh to the crack geometry and crack propagation without remeshing. The method can improve the accuracy by incorporating arbitrary functions into the displacement field of the standard FEM to describe the local behavior around the singular features such as crack tips, notches or corners and thus is a flexible and powerful tool in the field of fracture mechanics. Currently, the XFEM is widely used to simulate two- and three-dimensional elastic and plastic fracture problems [Elguedj et al. (2006); Bordas et al. (2008); Rabczuk et al. (2007); Rabczuk et al. (2009)]. Attracted by the advantages of the XFEM, researchers in other fields of computational physics have also employed it [Chessa et al. (2003); Chopp et al. (2003); Merle et al. (2002); Ji et al. (2002)].

On the other hand, a generalized gradient smoothing technique was introduced by [Chen et al. 2001]. More recently, Liu has established a G space theory and developed weakened weak (W2) formulation which has been the foundation for smoothed finite element methods (SFEM) [Liu et al. (2009); Liu (2010); Liu et al. (2010)]. Using different schemes of smoothing domain formation, cell-based smoothed finite element method (CS-FEM) [Le et al. (2010)], node-based smoothed finite element method (NS-FEM) [Liu et al. (2010)] and edge-based smoothed finite element method (ES-FEM) [Chen et al. (2012)] are developed. With the smoothing technique the domain integration is transformed into boundary integration according to the divergence theory. The shape function derivative is replaced with the shape function multiplied by the component of the outward unit vector along the boundary of the smoothing domain. Thanks to this transformation, the singular term existing in the derivatives of the shape functions for fracture mechanics is eliminated with smoothing technique. Smoothed methods have shown several advantages. For example, NS-FEM can provide upper bound solution [Liu et al. (2010)]. ES-FEM [Chen et al. (2012)] is proved to be more efficient and more accurate. In the ES-FEM, the system stiffness matrix is computed using strains smoothed over the smoothing domains formed based on the edges of the triangles. It is proved that the ES-FEM possesses the following excellent properties: (1) the ES-FEM model possesses a close-to-exact stiffness: it is much softer than the 'overly stiff' FEM and much stiffer than the 'overly soft' NS-FEM model; (2) the results are often found to be superconvergent and ultra-accurate: much more accurate than the linear triangular elements of FEM; (3) the implementation of the method is straightforward and no penalty parameter is used, and the computational efficiency is better than the FEM

using the same set of nodes. These properties of the ES-FEM have been confirmed by many works [[Chen et al. (2012)], Liu et al. (2008); Cui et al. (2011)].

In view of the advantages of XFEM and ES-FEM, an edge-based smoothed XFEM has been developed to combine the advantages of the two methods for two-dimensional fracture problems [Jiang et al. (2013); Chen et al. (2012)]. Although the ES-XFEM has achieved remarkable progress in the simulation of fracture mechanics, the previous works are confined to two-dimensional fracture problems. In this paper, for the first time, the face-based smoothing technique is combined into XFEM to develop three-dimensional face-based smoothed extended finite element method (FS-XFEM).

[Karihaloo et al. (2003); Karihaloo et al. (2001)] from a simplified variational function using a truncated asymptotic crack tip displacement, formulated the hybrid crack element (HCE) for evaluating the SIF but also the coefficients of the higher order terms of the crack tip. But it has not been extended to three-dimensional fracture problem. A direct traction boundary integral equation method (TBIEM) for three-dimensional crack problems is developed in [Xie et al. (2014)]. However, a singular system of equations is always obtained [Aliabadi (1997); Cruse (1988)]. Special methods [Pan (1997)] has to be employed to tackle this problem. The proposed FS-XFEM will not have these problems comparing with the above problems.

This paper is organized as follows: Section 2 provides a brief description of FS-FEM. Section 3 introduces the formation of face-based smoothed XFEM. Section 4 illustrates the computational procedure for three-dimensional stress intensity factor (SIF). Section 5 gives two examples to test the newly developed method and compare the results of FS-XFEM with those of XFEM. The conclusion is made in Section 6.

2. Face-based smoothed FEM (FS-FEM)

2.1. Smoothing domain formation

Due to the excellent features of ES-FEM in two-dimensional problems, the FS-FEM [Nguyen-Thoi et al. (2009a; 2009b)] for three-dimensional problems is developed. In the FS-FEM, linear tetrahedral elements, which are feasible for arbitrarily complicated geometry, are used to mesh the problem domain. Instead of using the edges of the elements in two-dimensional problems, faces of the elements in the FS-FEM are used to create smoothing domains. Therefore, it is named face-based smoothed finite element method. The faces of the elements in three-dimension can be classified into two types: boundary face and interior face. The boundary face lies on the boundary of the domain, while the interior face lies inside the domain. The smoothing domains associated with these two types of faces are formed in different ways. For the interior face, which is shared by two elements, the smoothing domain is formed by connecting the three points of the face to the centroids of the two elements shown in Fig. 1(a). For the boundary face, which belongs to only one element, the smoothing domain is formed by the face and the centroid of the only element. Four points (three from the face and one being the centroid of the element) automatically form a tetrahedral shown in Fig. 1(b).

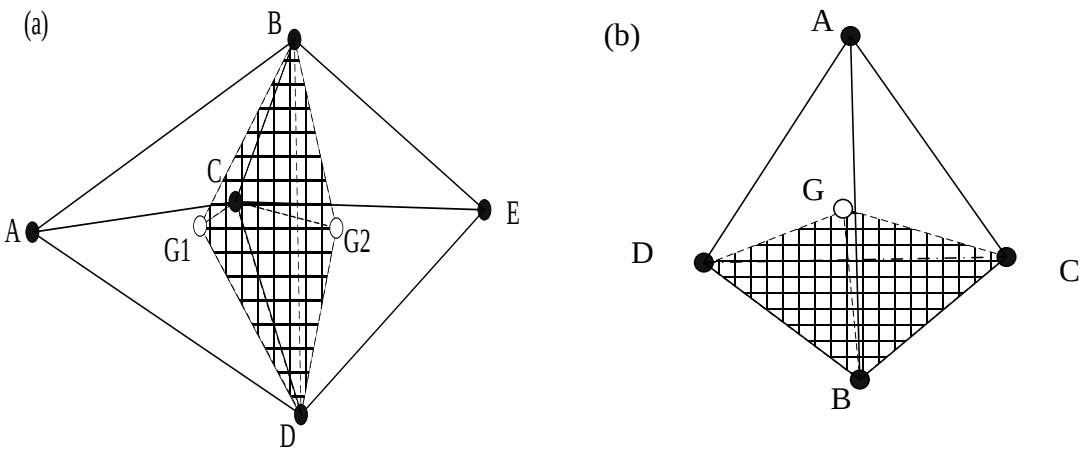

Figure 1. Two types of smoothing domains (a) smoothing domain formed based on interior face (b) smoothing domain formed based on boundary face

2.2. The formulation of FS-FEM

In the FS-FEM, the problem domain is meshed with 4-node tetrahedral elements. Based on the above description of smoothing domain formulation, N_{face} smoothing domains in the whole model can be created. Here N_{face} is the number of the faces in the whole problem domain Ω. The smoothing domains satisfy $\Omega = \sum_{k=1}^{N_{face}} \Omega^k$ and $\Omega^i \cap \Omega^j = \varnothing$, $i \neq j$. With face-based smoothing technique, the integration of the derivatives of the shape functions over domain can be transformed into integration of shape functions multiplied with component of outward unit vector of the boundary face. The integration result is then divided by the volume of the smoothing domain. In the setting of FS-FEM, the smoothed strain is obtained as:

$$\bar{\boldsymbol{\varepsilon}} = \bar{\mathbf{B}}\mathbf{u} \tag{1}$$

Here $\mathbf{u} = \begin{bmatrix} u_1 & v_1 & w_1 & \cdots & u_{ns} & v_{ns} & w_{ns} \end{bmatrix}^T$ is the displacement vector with all the displacement components of the nodes belonging to the smoothing domain. $\bar{\mathbf{B}}$ is the strain-displacement relationship matrix in three dimension expressed as:

$$\bar{\mathbf{B}} = \begin{bmatrix} \bar{b}_{ix}(\mathbf{x}_k) & 0 & 0 \\ 0 & \bar{b}_{iy}(\mathbf{x}_k) & 0 \\ 0 & 0 & \bar{b}_{iz}(\mathbf{x}_k) \\ \bar{b}_{iy}(\mathbf{x}_k) & \bar{b}_{ix}(\mathbf{x}_k) & 0 \\ 0 & \bar{b}_{iz}(\mathbf{x}_k) & \bar{b}_{iy}(\mathbf{x}_k) \\ \bar{b}_{iz}(\mathbf{x}_k) & 0 & \bar{b}_{ix}(\mathbf{x}_k) \end{bmatrix} \tag{2}$$

with

$$\bar{b}_{ih}(\mathbf{x}_k) = \frac{1}{V_k^s}\int_{\Gamma^k} n_h^k(\mathbf{x}) N_i(\mathbf{x}) d\Gamma \qquad h = (x, y, z) \tag{3}$$

where Γ^k is the boundary face of the smoothing domain. $n_h^k(\mathbf{x})$ is the h component of the outward normal vector on the boundary Γ^k. $N_i(\mathbf{x})$ is the shape function. V_k^s is the volume of the smoothing domain.

By Gauss quadrature, $\bar{b}_{ih}(\mathbf{x}_k)$ can be further written as:

$$\bar{b}_{ih}(\mathbf{x}_k) = \frac{1}{V_k^s}\sum_{m=1}^{N_{face}^k}\sum_{n=1}^{N_{gau}} n_h^k(\mathbf{x}_n) N_i(\mathbf{x}_n) w_n \; h = (x, y, z) \tag{4}$$

where N_{gau} is the number of the Gauss points and w_n is the weight of the Gauss point. N_{face}^k is the number of faces attached to the smoothing domain Ω^k. $\mathbf{x}_n$ is the coordinate of the Gauss point on the boundary face. $N_i(\mathbf{x}_n)$ is the ith shape function of the Gauss point $\mathbf{x}_n$. $n_n^k(\mathbf{x}_n)$ is the outward unit normal component.

The set of algebraic equations for FS-FEM can be obtained in the form of matrix:

$$\overline{\mathbf{K}}\overline{\mathbf{d}} = \mathbf{f} \tag{5}$$

Here $\bar{\mathbf{d}}$ is the displacement vector of all the nodes in the model, $\overline{\mathbf{K}}$ is the global stiffness matrix and $\mathbf{f}$ is the nodal force.

The entries in sub-matrices of the stiffness matrix $\overline{\mathbf{K}}$ in Eq. (5) can be expressed as:

$$\overline{\mathbf{K}}_{ij} = \sum_{k=1}^{N_{face}} \overline{\mathbf{K}}_{ij,k}^s \tag{6}$$

Here the summation means an assembly process, $\overline{\mathbf{K}}_{ij,k}^s$ is the stiffness matrix associated with the smoothing domain Ω^k and can be computed by

$$\overline{\mathbf{K}}_{ij,k}^s = \int_{\Omega_k^s} \overline{\mathbf{B}}_i^{\mathrm{T}} \mathbf{D} \overline{\mathbf{B}}_j d\Omega = \overline{\mathbf{B}}_i^{\mathrm{T}} \mathbf{D} \overline{\mathbf{B}}_j V_k^s \tag{7}$$

where V_k^s is the volume of the smoothing domain Ω^k, $\mathbf{D}$ is the matrix of material constants that is defined as follows:

$$\mathbf{D}=\begin{bmatrix} 2G+\lambda & \lambda & \lambda & 0 & 0 & 0 \\ \lambda & 2G+\lambda & \lambda & 0 & 0 & 0 \\ \lambda & \lambda & 2G+\lambda & 0 & 0 & 0 \\ 0 & 0 & 0 & G & 0 & 0 \\ 0 & 0 & 0 & 0 & G & 0 \\ 0 & 0 & 0 & 0 & 0 & G \end{bmatrix} \tag{8}$$

with $G=\dfrac{E}{2(1+\nu)}$, $\lambda=\dfrac{\upsilon E}{(1+\nu)(1-2\nu)}$. Here E is the Young's modulus, and ν is the Poisson's ratio.

3. Face-based smoothed XFEM (FS-XFEM)

3.1. The formulation of FS-XFEM

The displacement of XFEM is composed of three parts: the continuous displacement from standard finite element method, the enrichment part that represents discontinuity across the crack surface and the enrichment part that describes the singular strain field around the crack front. Heaviside function is usually employed as enrichment function for the discontinuity across the crack surface. A set of branch functions, which are derived from the displacement field around the crack front, are used to produce the singular strain field around the crack front. Nodal subtraction is used in FS-XFEM.

$$\begin{aligned} u(\mathbf{x}) = & \sum_{i\in N^{fs-fem}} N_i(\mathbf{x})u_i + \sum_{j\in N^{fs-c}} N_j(H(\mathbf{x})-H(\mathbf{x}_j))a_j \\ & + \sum_{k\in N^{fs-e}} N_k(\mathbf{x})\sum_{\alpha=1}^{4}(\phi_\alpha(\mathbf{x})-\phi_\alpha(\mathbf{x}_k))b_k^\alpha \end{aligned} \tag{9}$$

Here $N_i(x)$, $N_j(x)$ and $N_k(x)$ are the shape functions associated with different types of nodes and u_i is nodal displacement in standard FEM. N^{fs-fem} is the node set of the whole finite element model. $\mathbf{x}_j$ and $\mathbf{x}_k$ are the coordinates of the jth and kth nodes in the element respectively. $H(\mathbf{x})$ is a Heaviside jump function and is set as follows:

$$H(\mathbf{x})=\begin{cases} 1 & \text{if } (\mathbf{x}-\mathbf{x}^*)\cdot\mathbf{n}\geq 0 \\ -1 & \text{otherwise} \end{cases} \tag{10}$$

N^{fs-c} is the set of nodes whose support domain is completely cut by the crack surface. a_j is the enriched degree of freedom associated with node set N^{fs-c}. N^{fs-e} is the set of nodes in the vicinity of the crack front. $\phi_\alpha(\mathbf{x})$ are a set of branch functions to model the asymptotic features of the displacement field around the crack front:

$$\phi_\alpha(\mathbf{x})(\alpha = 1-4)$$
$$= \left\{ \sqrt{r}\sin(\frac{\theta}{2}) \quad \sqrt{r}\cos(\frac{\theta}{2}) \quad \sqrt{r}\sin(\frac{\theta}{2})\sin(\theta) \quad \sqrt{r}\cos(\frac{\theta}{2})\sin(\theta) \right\} \tag{11}$$

where (r,θ) is the local polar coordinate system, which is defined so that the plane where $\theta = 0$ must be tangent to the crack front. b_k^α is the αth (of the totally four) enriched degree of freedom associated with node set N^{fs-e}.

Caused by different types of enrichment functions, nodes in FS-XFEM can be categorized into three types. (a) common nodes denoted by N^{fs-fem}, which are not enriched by either $H(\mathbf{x})$ or $\phi_\alpha(\mathbf{x})$; (b) $\phi_\alpha(\mathbf{x})$ enriched nodes denoted by N^{fs-e}. As shown in Fig. 2(a), the smoothing domain $ABCG_1G_2$. Here ABC is the face, based on which the smoothing domain is formed. G_1 and G_2 are the centroids of the two elements, which share the face ABC. The crack surface $EFMN$ is in this smoothing domain. But the crack front MN is also inside the smoothing domain, which means that the crack surface does not completely cut the smoothing domain but part of the smoothing domain. $\phi_\alpha(\mathbf{x})$ is used to describe the displacement behavior around the crack front. Therefore, nodes associated with this smoothing domain are enriched by $\phi_\alpha(\mathbf{x})$. (c) $H(\mathbf{x})$ enriched nodes denoted by N^{fs-c}. As shown in Fig. 2(b), the smoothing domain $ABCG_1G_2$ is constructed in the same way as Fig. 2(a). Here EFD is the crack surface. This smoothing domain is completely cut by the crack surface. Therefore, $H(\mathbf{x})$ is used to enrich the nodes associated with the smoothing domain, if the nodes are not enriched by $\phi_\alpha(\mathbf{x})$.

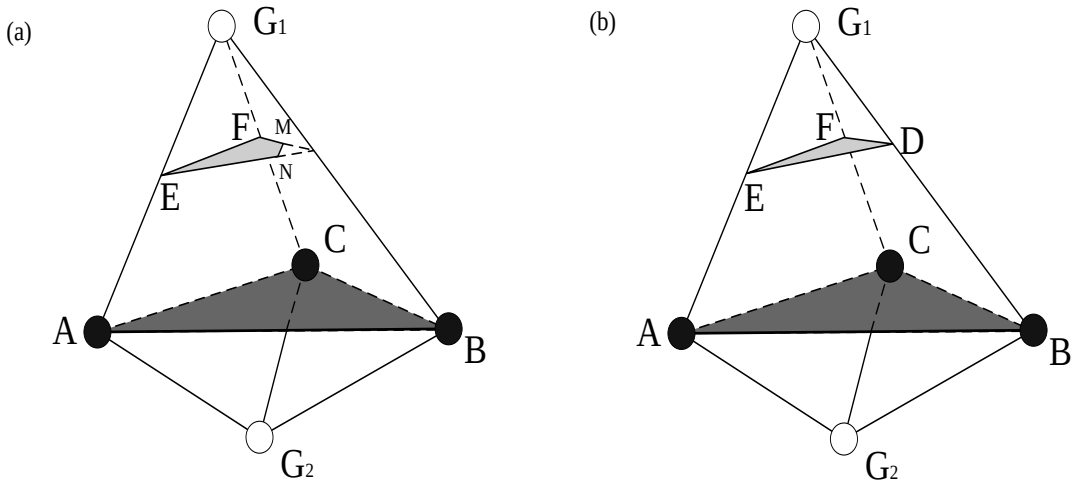

Figure 2. (a) crack-front element (b) crack-cut element

Employing the strain smoothing operation, the smoothed strain over Ω^k from the displacement approximation can be written as:

$$\bar{\boldsymbol{\varepsilon}}_k(\mathbf{x}) = \sum_{i\in N^{fs-fem}} \bar{\mathbf{B}}_i^u(\mathbf{x}_k)\mathbf{u}_i + \sum_{j\in N^{fs-c}} \bar{\mathbf{B}}_j^a(\mathbf{x}_k)\mathbf{a}_j + \sum_{m\in N^{fs-e}} \bar{\mathbf{B}}_m^b(\mathbf{x}_k)\sum_{\alpha=1}^{4} b_k^\alpha \tag{12}$$

where $\bar{\mathbf{B}}_i^u(\mathbf{x}_k)$ is the smoothed strain gradient matrix for the standard FS-FEM part, and $\bar{\mathbf{B}}_j^a(\mathbf{x}_k)$, $\bar{\mathbf{B}}_m^b(\mathbf{x}_k)$ correspond to the Heaviside function and branch functions enriched parts respectively. Those matrices can be written as:

$$\bar{\mathbf{B}}_i^r(\mathbf{x}_k) = \begin{bmatrix} \bar{b}_{ix}^r(\mathbf{x}_k) & 0 & 0 \\ 0 & \bar{b}_{iy}^r(\mathbf{x}_k) & 0 \\ 0 & 0 & \bar{b}_{iz}^r(\mathbf{x}_k) \\ \bar{b}_{iy}^r(\mathbf{x}_k) & \bar{b}_{ix}^r(\mathbf{x}_k) & 0 \\ 0 & \bar{b}_{iz}^r(\mathbf{x}_k) & \bar{b}_{iy}^r(\mathbf{x}_k) \\ \bar{b}_{iz}^r(\mathbf{x}_k) & 0 & \bar{b}_{ix}^r(\mathbf{x}_k) \end{bmatrix} \tag{13}$$

In the above equation, $\bar{b}_{ih}^r(\mathbf{x}_k), h = x, y, z$ and $r = u, a, b$ is computed by:

$$\begin{aligned} \bar{b}_{ih}^u(\mathbf{x}_k) &= \frac{1}{V_k^s}\int_{\Gamma^k} n_h(\mathbf{x})N_i(\mathbf{x})d\Gamma \\ \bar{b}_{ih}^a(\mathbf{x}_k) &= \frac{1}{V_k^s}\int_{\Gamma^k} n_h(\mathbf{x})N_i(\mathbf{x})(H(\mathbf{x}) - H(\mathbf{x}_i))d\Gamma \qquad (h = x, y, z) \\ \bar{b}_{ih}^b(\mathbf{x}_k) &= \frac{1}{V_k^s}\int_{\Gamma^k} n_h(\mathbf{x})N_i(\mathbf{x})(\phi_\alpha(\mathbf{x}) - \phi_\alpha(\mathbf{x}_i))d\Gamma \end{aligned} \tag{14}$$

Using Gauss quadrature along the segments of boundary, the above equations can be written as:

$$\begin{aligned} \bar{b}_{ih}^u(\mathbf{x}_k) &= \frac{1}{V_k^s}\sum_{m=1}^{N_{face}^k}\sum_{n=1}^{N_{gau}} n_h(\mathbf{x}_n)N_i(\mathbf{x}_n)w_n \\ \bar{b}_{ih}^a(\mathbf{x}_k) &= \frac{1}{V_k^s}\sum_{m=1}^{N_{face}^k}\sum_{n=1}^{N_{gau}} n_h(\mathbf{x}_n)N_i(\mathbf{x}_n)(H(\mathbf{x}_n) - H(\mathbf{x}_i))w_n \qquad (h = x, y, z) \\ \bar{b}_{ih}^b(\mathbf{x}_k) &= \frac{1}{V_k^s}\sum_{m=1}^{N_{face}^k}\sum_{n=1}^{N_{gau}} n_h(\mathbf{x}_{m,n})N_i(\mathbf{x}_n)(\phi_\alpha(\mathbf{x}_n) - \phi_\alpha(\mathbf{x}_i))w_n \end{aligned} \tag{15}$$

Here N_{face}^k is the number of the boundary faces of the smoothing domain, N_{gau} is the number of the Gauss points used on the boundary face. $\mathbf{x}_n$ is the coordinate of the nth Gauss point on the boundary face.

The stiffness matrix $\overline{\mathbf{K}}$ is yielded by:

$$\begin{aligned}\overline{\mathbf{K}}_{ij} &= \sum_{k=1}^{N_s} \overline{\mathbf{K}}_{ij,k}^{s} \\ &= \sum_{k=1}^{N_s} \begin{bmatrix} (\overline{\mathbf{B}}_i^u)^T \mathbf{D} \overline{\mathbf{B}}_j^u V_k^s & (\overline{\mathbf{B}}_i^u)^T \mathbf{D} \overline{\mathbf{B}}_j^a V_k^s & (\overline{\mathbf{B}}_i^u)^T \mathbf{D} \overline{\mathbf{B}}_j^b V_k^s \\ (\overline{\mathbf{B}}_i^a)^T \mathbf{D} \overline{\mathbf{B}}_j^u V_k^s & (\overline{\mathbf{B}}_i^a)^T \mathbf{D} \overline{\mathbf{B}}_j^a V_k^s & (\overline{\mathbf{B}}_i^a)^T \mathbf{D} \overline{\mathbf{B}}_j^b V_k^s \\ (\overline{\mathbf{B}}_i^b)^T \mathbf{D} \overline{\mathbf{B}}_j^u V_k^s & (\overline{\mathbf{B}}_i^b)^T \mathbf{D} \overline{\mathbf{B}}_j^a V_k^s & (\overline{\mathbf{B}}_i^b)^T \mathbf{D} \overline{\mathbf{B}}_j^b V_k^s \end{bmatrix} \end{aligned} \tag{16}$$

Substituting Eq. (16) into Eq. (5) can produce a set of linear equations. In FS-XFEM, $\mathbf{f}$ is composed of three parts: $\mathbf{f}^u, \mathbf{f}^a$ and $\mathbf{f}^b$. These three vectors can be obtained as follows:

$$\begin{aligned} \mathbf{f}_{i,m}^{u} &= \int_{\Omega_m^e} N_i(\mathbf{x}) \mathbf{b} d\Omega + \int_{\Gamma_t} N_i(\mathbf{x}) \mathbf{t}_\Gamma d\Gamma \\ \mathbf{f}_{i,m}^{a} &= \int_{\Omega_m^e} N_i(\mathbf{x}) H(\mathbf{x}) \mathbf{b} d\Omega + \int_{\Gamma_t} N_i(\mathbf{x}) H(\mathbf{x}) \mathbf{t}_\Gamma d\Gamma \\ \mathbf{f}_{i,m}^{b\alpha} &= \int_{\Omega_m^e} N_i(\mathbf{x}) \phi_\alpha(\mathbf{x}) \mathbf{b} d\Omega + \int_{\Gamma_t} N_i(\mathbf{x}) \phi_\alpha(\mathbf{x}) \mathbf{t}_\Gamma d\Gamma \end{aligned} \tag{17}$$

4. Three-dimensional stress intensity factor calculation

Several numerical techniques, in conjunction with finite-element (FE) analyses, have been developed to calculate fracture mechanics parameters. Three of these techniques are: (1) the virtual crack extension (VCE) method [Parks et al. (1974; 1977); Hellen (1975; 1989)], (2) the virtual crack closure technique [Rybicki et al. (1977); Shivakumar et al.(1988); Raju et al. (1988); Buchholz (1984)], and (3) the *J*-integral method [Rice (1968); Cherepanov (1967; 1969); Eshelby (1956);]. Based on *J*-integral method, an interaction energy integral method is used to calculate stress intensity factor in this work. A cylindrical volume with the radius r_d surrounding a point C located on the crack front is shown in Fig. 3. If the crack surfaces are traction-free, the domain form of the interaction energy integral $I(s)$ can be written as:

$$I(s) = \frac{-\int_V [\mathrm{tr}(\mathbf{P} \cdot \vec{\nabla} \mathbf{q}) + (\vec{\nabla} \cdot \mathbf{P}^{\mathrm{T}}) \cdot \mathbf{q}] dV}{\int_{L_c} \Delta a(s) ds} \tag{18}$$

where

$$\mathbf{P} = \boldsymbol{\sigma} : \boldsymbol{\varepsilon}^{\mathrm{aux}} \mathbf{I} - \vec{\nabla} \mathbf{u}^{\mathrm{aux}} \cdot \boldsymbol{\sigma} - \vec{\nabla} \mathbf{u} \cdot \boldsymbol{\sigma}^{\mathrm{aux}} \tag{19}$$

Here the superscript aux stands for auxiliary field. $\boldsymbol{\varepsilon}$, $\mathbf{u}$ and $\boldsymbol{\sigma}$ are the actual strain, displacement and stress field respectively.

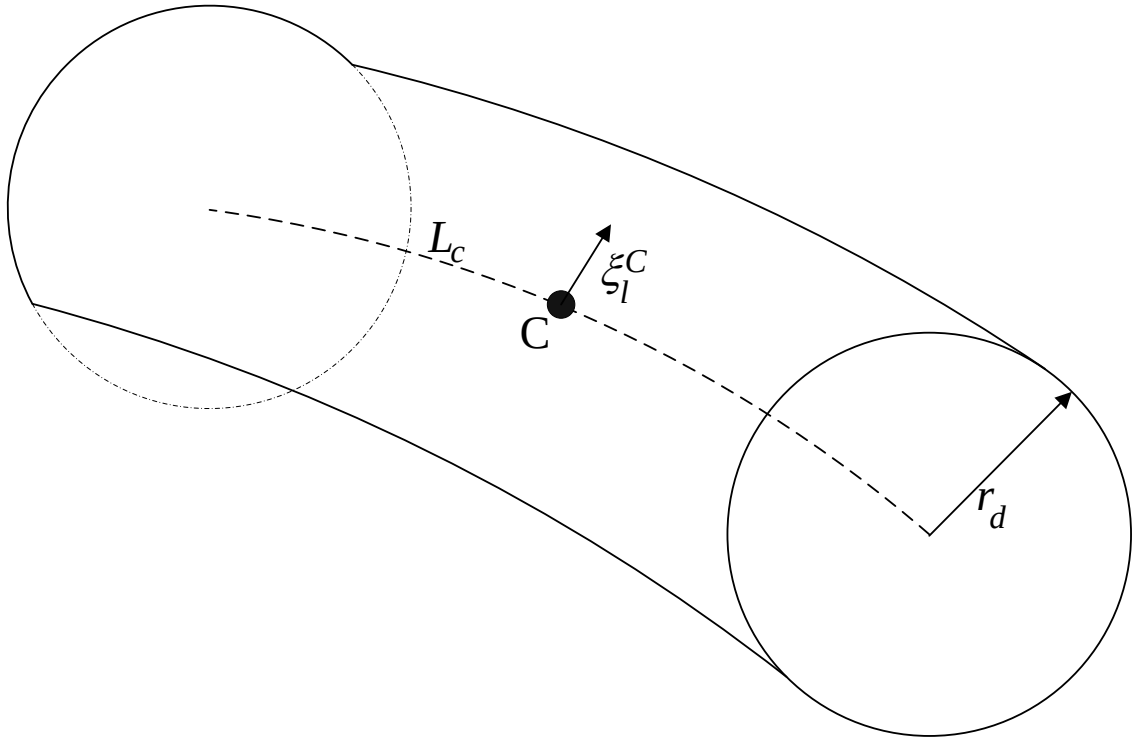

Figure. 3. A cylindrical volume surrounding a point C

The main difficulty in the calculation of interaction energy integral lies in the evaluation of the gradients and higher order gradients of the auxiliary fields that appear in the integrand. As shown in Fig. 4, we define a local orthogonal coordinate system at a point s along the crack front such that the local x_2 axis is perpendicular to the plane of the crack, and the x_1 and x_3 axes lie in the plane of the crack and are normal and tangent respectively to the crack front. To illustrate a convenient procedure to evaluate these gradients, we consider a point p which lies in the local $x_1 - x_2$ plane as shown in Fig. 4. The base vectors $\mathbf{e}_1$, $\mathbf{e}_2$ and $\mathbf{e}_3$ as shown in the figure are constructed by keeping $\mathbf{e}_1$ and $\mathbf{e}_2$ parallel to x_1 and x_2 and moving in the direction of x_3. r, θ are local polar coordinates defined in the figure. The auxiliary fields expressed in this orthogonal curvilinear coordinate system are given as:

$$
\begin{aligned}
\sigma_{11}^{\text{aux}} &= \frac{1}{\sqrt{2\pi r}}\left\{K_{\text{I}}^{\text{aux}}\cos\frac{\theta}{2}\left[1-\sin\frac{\theta}{2}\sin\frac{3\theta}{2}\right]-K_{\text{II}}^{\text{aux}}\sin(\frac{\theta}{2})\left[2+\cos\frac{\theta}{2}\cos\frac{3\theta}{2}\right]\right\}\\
\sigma_{22}^{\text{aux}} &= \frac{1}{\sqrt{2\pi r}}\left\{K_{\text{I}}^{\text{aux}}\cos\frac{\theta}{2}\left[1+\sin\frac{\theta}{2}\sin\frac{3\theta}{2}\right]+K_{\text{II}}^{\text{aux}}\sin\frac{\theta}{2}\cos\frac{\theta}{2}\cos\frac{3\theta}{2}\right\}\\
\sigma_{12}^{\text{aux}} &= \frac{1}{\sqrt{2\pi r}}\left\{K_{\text{I}}^{\text{aux}}\sin\frac{\theta}{2}\cos\frac{\theta}{2}\cos\frac{3\theta}{2}+K_{\text{II}}^{\text{aux}}\cos\frac{\theta}{2}\left[1-\sin\frac{\theta}{2}\sin\frac{3\theta}{2}\right]\right\}\\
\sigma_{23}^{\text{aux}} &= \frac{K_{\text{III}}^{\text{aux}}}{\sqrt{2\pi r}}\cos\frac{\theta}{2}\\
\sigma_{13}^{\text{aux}} &= -\frac{K_{\text{III}}^{\text{aux}}}{\sqrt{2\pi r}}\sin\frac{\theta}{2}\\
\sigma_{33}^{\text{aux}} &= \upsilon(\sigma_{11}^{\text{aux}}+\sigma_{22}^{\text{aux}})
\end{aligned}
\tag{20}
$$

$$
\begin{aligned}
u_1^{\text{aux}} &= \frac{1}{8G}\sqrt{\frac{2r}{\pi}}\left\{K_{\text{I}}^{\text{aux}}\left[(5-8\upsilon)\cos\frac{\theta}{2}-\cos\frac{3\theta}{2}\right]+K_{\text{II}}^{\text{aux}}\left[(9-8\upsilon)\sin\frac{\theta}{2}+\sin\frac{3\theta}{2}\right]\right\}\\
u_2^{\text{aux}} &= \frac{1}{8G}\sqrt{\frac{2r}{\pi}}\left\{K_{\text{I}}^{\text{aux}}\left[(7-8\upsilon)\sin\frac{\theta}{2}-\sin\frac{3\theta}{2}\right]-K_{\text{II}}^{\text{aux}}\left[(3-8\upsilon)\cos\frac{\theta}{2}+\cos\frac{3\theta}{2}\right]\right\}\\
u_3^{\text{aux}} &= \frac{1}{G}\sqrt{\frac{2r}{\pi}}K_{\text{III}}^{\text{aux}}\sin\frac{\theta}{2}
\end{aligned}
\tag{21}
$$

$$
\begin{aligned}
&\varepsilon_{11}^{\text{aux}} = \frac{\partial u_1^{\text{aux}}}{\partial\xi_1};\ \varepsilon_{22}^{\text{aux}} = \frac{\partial u_2^{\text{aux}}}{\partial\xi_2};\ \varepsilon_{12}^{\text{aux}} = \frac{1}{2}(\frac{\partial u_2^{\text{aux}}}{\partial\xi_1}+\frac{\partial u_1^{\text{aux}}}{\partial\xi_1})\\
&\varepsilon_{13}^{\text{aux}} = \frac{1}{2}(\frac{\partial u_1^{\text{aux}}}{\partial\xi_3}+\frac{\partial u_3^{\text{aux}}}{\partial\xi_1});\ \varepsilon_{23}^{\text{aux}} = \frac{1}{2}(\frac{\partial u_3^{\text{aux}}}{\partial\xi_2}+\frac{\partial u_2^{\text{aux}}}{\partial\xi_3});\ \varepsilon_{33}^{\text{aux}} = 0
\end{aligned}
\tag{22}
$$

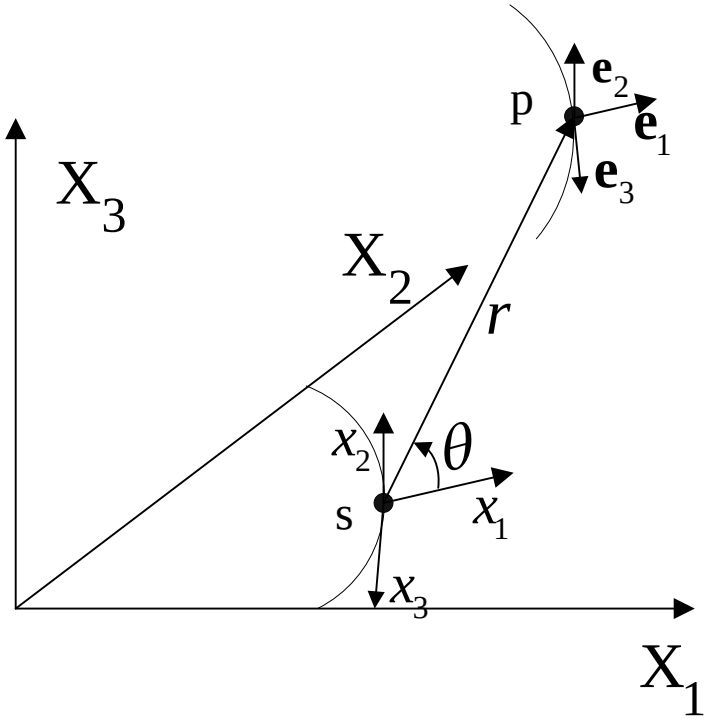

Figure 4. Local orthogonal coordinate system at a point s along the crack front

The weighting function q is defined as follows: A set of elements having at least one node within a cylindrical volume of radius r_d around the crack front are selected. The value of q_c of node associated with the crack tip C is defined:

$$q_c = \begin{cases} \xi_l^C & \text{if } x_3^C = 0 \text{ and } r^C < r_d \\ 0 & \text{otherwise} \end{cases} \tag{23}$$

where ξ_l^C is a unit vector that is perpendicular to the crack front at the crack tip C and lies in the local tangent plane to the crack surface.

Having defined the auxiliary fields, the interaction energy integral $I(s)$ defined by Eq. (18) takes the value

$$I(s) = \frac{2(1-\upsilon^2)}{E}\left[K_{\mathrm{I}}K_{\mathrm{I}}^{\mathrm{aux}} + K_{\mathrm{II}}K_{\mathrm{II}}^{\mathrm{aux}}\right] + \frac{1}{G}K_{\mathrm{III}}K_{\mathrm{III}}^{\mathrm{aux}} \tag{24}$$

Here $K_{\mathrm{I}}^{\mathrm{aux}}$, $K_{\mathrm{II}}^{\mathrm{aux}}$, and $K_{\mathrm{III}}^{\mathrm{aux}}$ are the stress intensity factors associated with the auxiliary fields and K_{I}, K_{II}, and K_{III} are the stress intensity factors associated with the actual fields. The process of evaluating the actual stress intensity factors involves making a judicious choice of the auxiliary stress intensity factors, and then evaluating the interaction energy integral. For example, Substituting $K_{\mathrm{I}}^{\mathrm{aux}} = 1$, and $K_{\mathrm{II}}^{\mathrm{aux}} = K_{\mathrm{III}}^{\mathrm{aux}} = 0$ into Eq. (24) yields:

$$K_{\mathrm{I}}(s)=\frac{E}{2(1-\upsilon^2)}I(s) \tag{25}$$

Similarly, K_{II} can be obtained by substituting $K_{\mathrm{II}}^{\mathrm{aux}}=1$ and $K_{\mathrm{I}}^{\mathrm{aux}}=K_{\mathrm{III}}^{\mathrm{aux}}=0$ and K_{III} by substituting $K_{\mathrm{III}}^{\mathrm{aux}}=1$ and $K_{\mathrm{I}}^{\mathrm{aux}}=K_{\mathrm{II}}^{\mathrm{aux}}=0$.

5. Numerical examples

Two examples are presented in this work to test our method. One is a plate with a thorough edge crack under tension. The other problem is a cylinder with a penny-shaped crack under remote tension. Strain energy and SIFs are obtained by FS-XFEM and compared with those of XFEM.

5.1. A plate with a thorough edge crack under tension

A plate with a thorough edge crack under tension is first analyzed as shown in Fig. 5. The mesh is plotted in Fig. 6. The dimension of plate is: the height $H=2\mathrm{mm}$ the width $W=1\mathrm{mm}$ and the thickness $t=0.5\mathrm{mm}$ with the crack length $a=0.3\mathrm{mm}$. The load $\sigma=1\mathrm{MPa}$ is applied on the top surface of the plate. All the degrees of freedom on the bottom surface are fixed. The material parameters are: Young's modulus $E=1\mathrm{MPa}$ and the Poisson's ratio $\upsilon=0.3$.

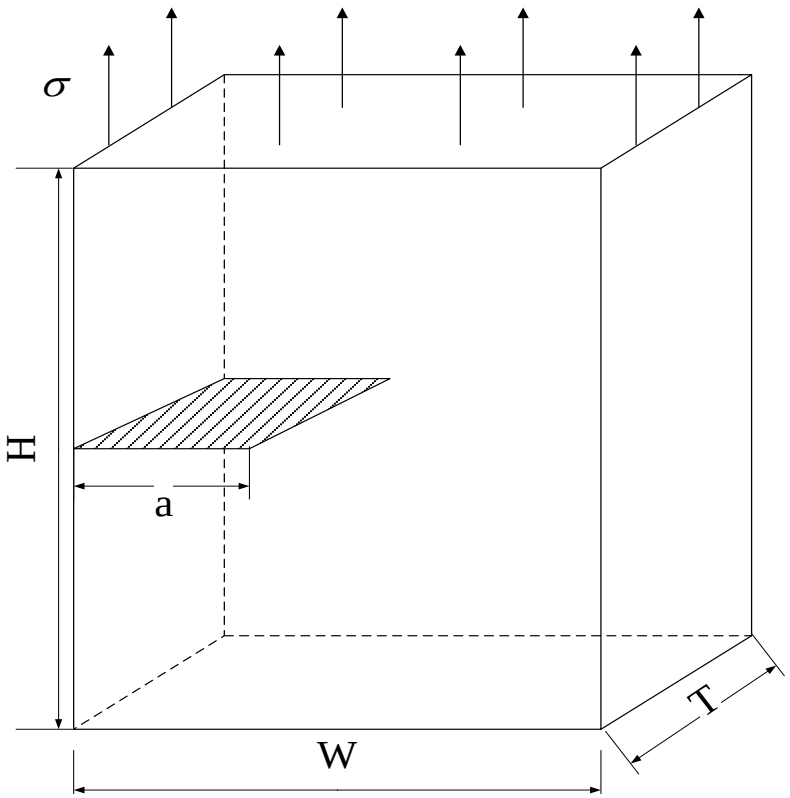

Figure 5. A plate with a thorough edge crack under tension

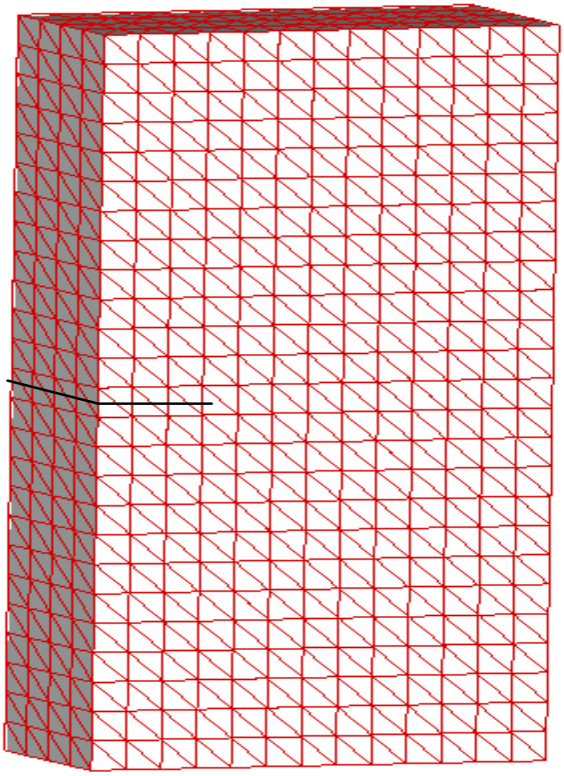

Figure 6. Mesh of the plate with a thorough edge crack

5.1.1 Result

Five types of meshes with linear tetrahedral elements ($13\times25\times4$, $18\times35\times4$, $19\times37\times4$, $31\times61\times4$, $41\times81\times4$) are used in the model. A sample mesh is shown in Fig. 6. For comparison, the results are also computed using XFEM. The reference solution of strain energy is obtained using singular FEM with very fine mesh (2,179,458 nodes) in this study. The strain energy is defined as:

$$U = \frac{1}{2}\int_{\Omega} \boldsymbol{\varepsilon}^T \mathbf{D}\boldsymbol{\varepsilon} d\Omega \tag{26}$$

The results of the strain energy produced by FS-XFEM and XFEM are plotted in Fig. 7. From the figure, it can be seen that the numerical results obtained from FS-XFEM are closer to the reference solution than those of XFEM using the same mesh. This is due to integration of face-based smoothing technique into the XFEM.

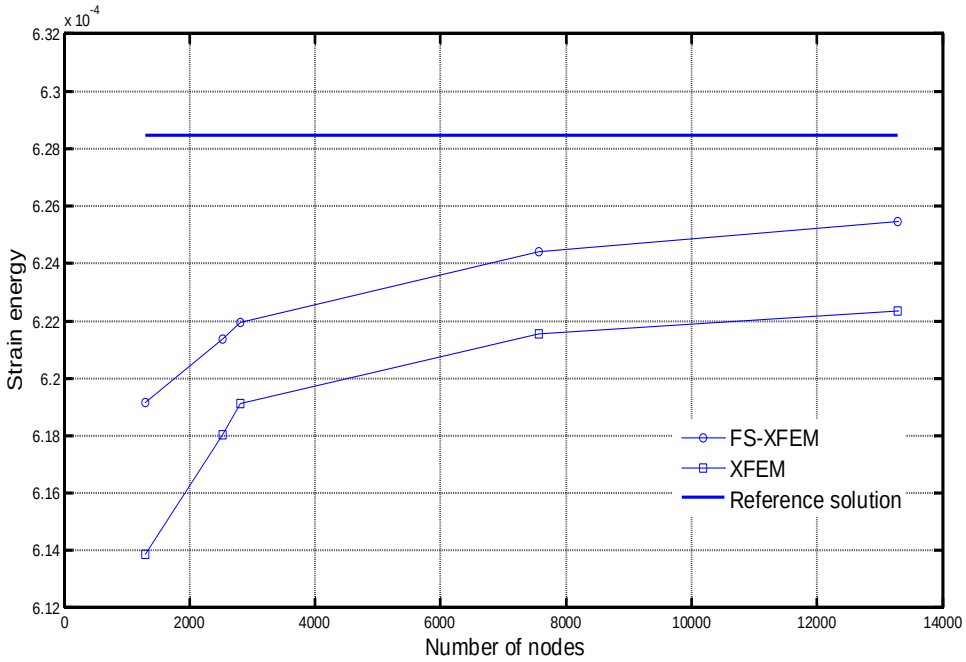

Figure 7. Plate with a thorough edge crack under tension: the variation of strain energy given by XFEM and FS-XFEM with different node numbers

5.1.2 Convergence rate of FS-XFEM

The convergence property of FS-XFEM and XFEM is studied in this section. In order to investigate quantitatively the numerical results, an error indicator in energy norm is defined as follows:

$$E_e = \sqrt{\frac{\left|U_{\text{num}} - U_{\text{ref}}\right|}{U_{\text{ref}}}} \tag{27}$$

where U_{ref} denotes the strain energy of reference solution and U_{num} stands for the strain energy of numerical solution. The errors in strain energy norm against h for this example is plotted in Fig. 8, where h is the average distance between two adjacent nodes. From the figure, it can be seen that the error of FS-XFEM is smaller than that of XFEM with the same mesh. At the same time, FS-XFEM has higher convergence rate than XFEM for this example, which means that FS-XFEM can converge to the reference solution at a higher rate.

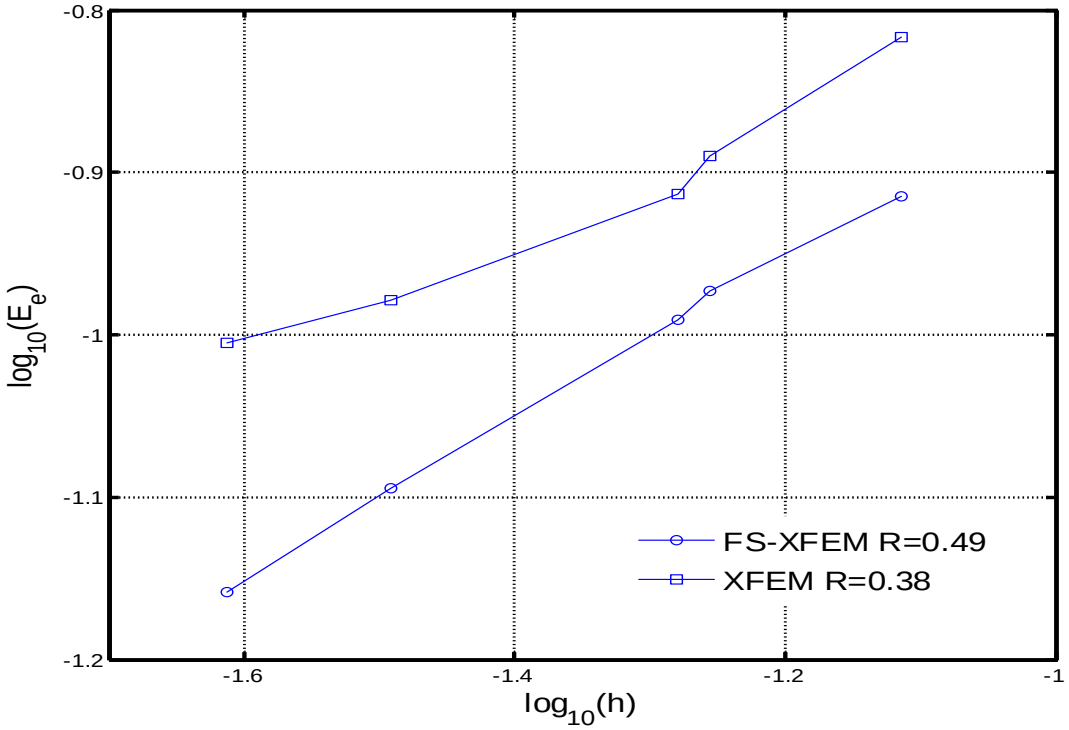

Fig. 8. Convergence rate of XFEM and ES-XFEM for a plate with a thorough crack under tension

5.1.3 Condition number

Another important property of numerical methods is the condition number of the global stiffness matrix, $cond(K)$. The condition number of the global stiffness matrix can affect the number of iterations needed to obtain a converged solution in the manner of $n_{iter} \propto \sqrt{cond(K)}$, when an iteration solver is used to solve the algebraic system equation. The condition number of FS-XFEM and XFEM for thist example against node numbers is listed in Table 1. As it can be seen, FS-XFEM has bigger condition number than XFEM with the same mesh. But the difference is not quite big.

Table 1. Condition numbers of FS-XFEM and XFEM for the first example with different mesh densities

Mesh	13×25×4	18×35×4	31×61×4	41×81×4
XFEM	1.3212e+006	1.8420e+006	1.4312e+007	1.7578e+007
FS-XFEM	1.5427e+006	2.0628e+006	1.7675e+007	2.8165e+007

5.1.4 Efficiency of FS-XFEM

In the assessment of numerical methods, the time cost of different numerical methods should also be taken into consideration. As shown in Table 2, the time consumption for FS-XFEM and XFEM with different meshes is compared. From the table, it is clear that the FS-XFEM takes more time to solve the equation than XFEM for the same mesh. This is in agreement with the condition number comparison between FS-XFEM and XFEM. However, after taking the results accuracy into account and

considering the efficiency, the present FS-XFEM is found to perform much better than XFEM for the results in energy error norms as shown in Fig. 9. From the figure, it is clear that within the same computation time, the results of FS-XFEM are more accurate than XFEM.

Table 2. Time cost of FS-XFEM and XFEM for the first example with different mesh densities

Mesh	13×25×4	18×35×4	31×61×4	41×81×4
XFEM	0.321761s	1.185841s	12.08005s	29.681937s
FS-XFEM	0.67652s	2.579944s	34.70061s	104.7701s

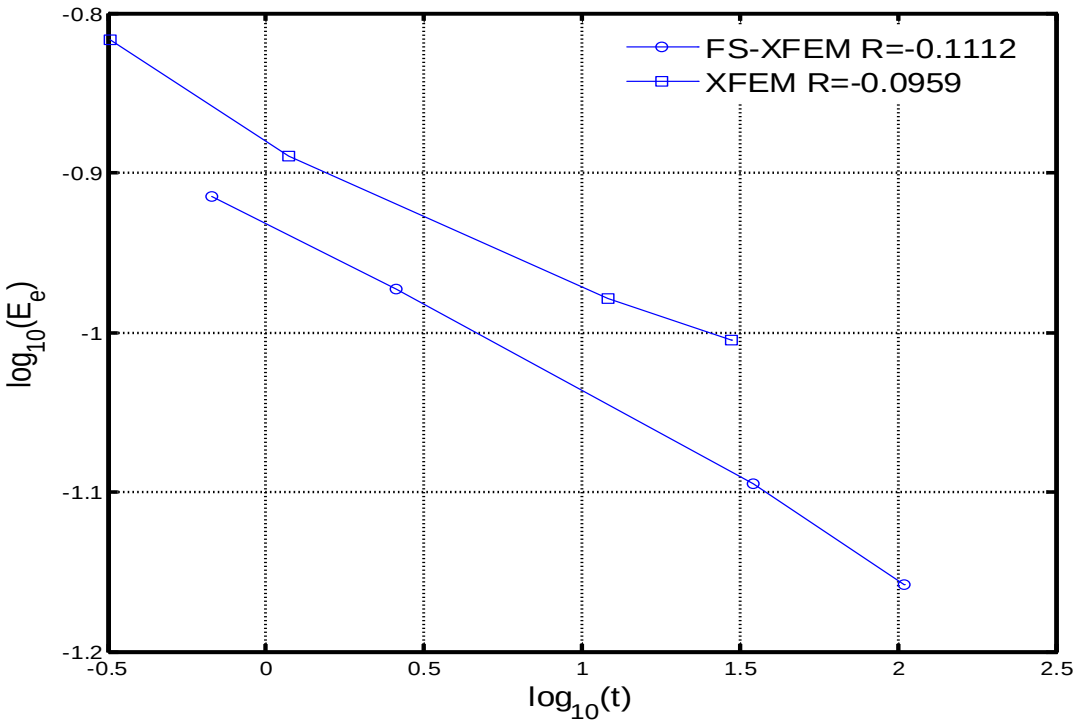

Figure 9. Comparison of computational efficiency of FS-XFEM and XFEM in terms of energy norm for a plate with a thorough crack under tension

5.2. A cylinder with a penny-shaped crack under remote tension

From the first example, it is seen that the FS-XFEM is powerful to simulate a straight crack in three-dimension. In order to extend the applicability of the proposed method, a cylinder with a penny-shaped crack under remote tension is studied. The crack is in the middle of the cylinder, with the radius (of the penny) $a = 0.3\,\text{mm}$ shown in Fig. 10. The remote tension is applied on the top surface of the cylinder. The bottom surface of the cylinder is fixed. The geometrical details are as follows: $H = 12\,\text{mm}$ and $R = 3\,\text{mm}$. With the ratio $a/R = 0.1$, this problem can be considered as a crack in an infinite body. The solution of stress intensity factor is given by [Anderson

(1995)]: $K_I = \frac{2}{\pi}\sigma\sqrt{\pi a}$. This is an axisymmetric problem. Due to the symmetry, only one quarter of the model is simulated with appropriate boundary condition shown in Fig. 11. In this model, symmetrical boundary condition are prescribed on both of the two side surfaces of the quarter-cylinder.

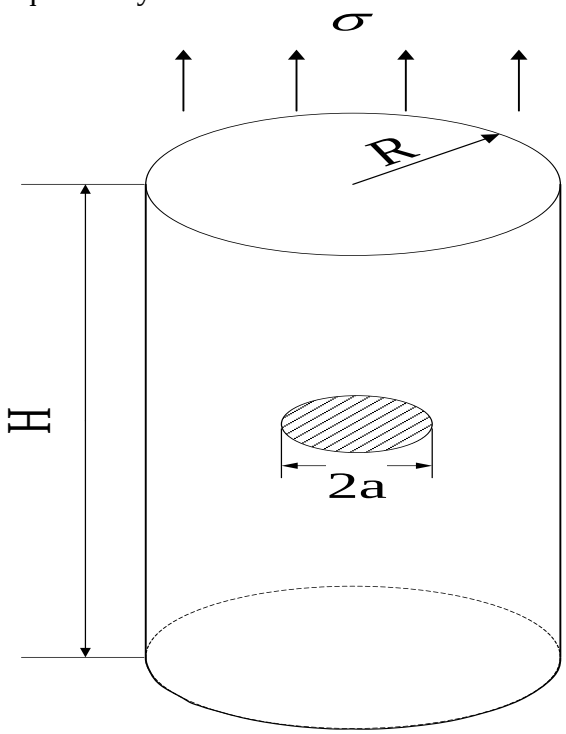

Figure 10. A cylinder with a penny-shaped crack under remote tension

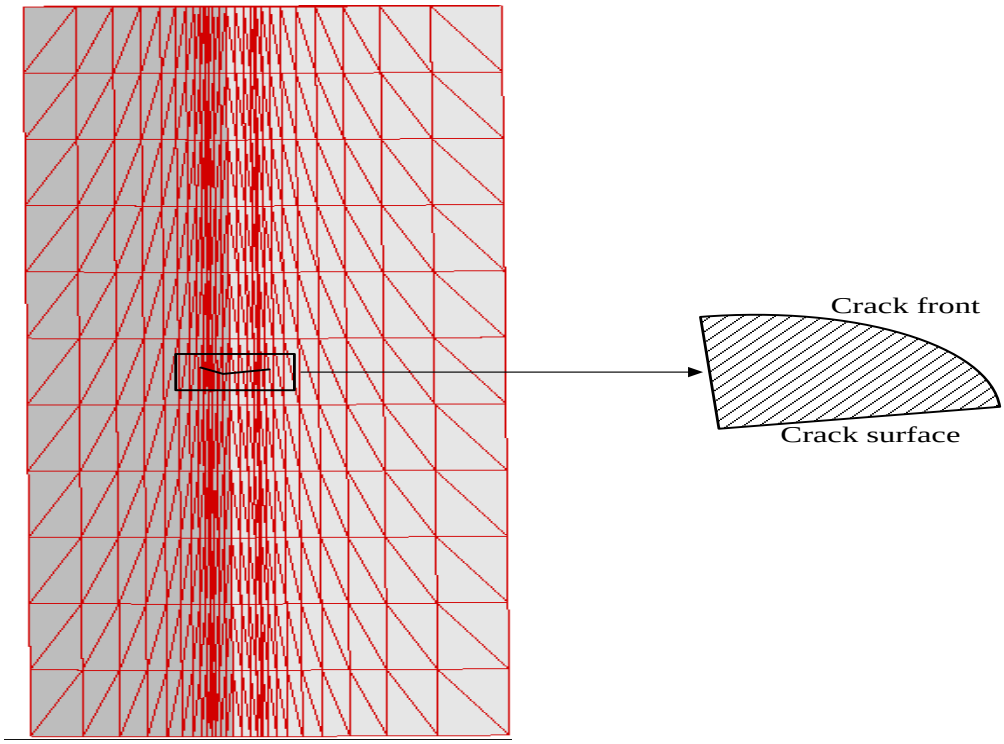

Figure 11. The mesh used for a cylinder with a penny-shaped crack under remote tension

The strain energy for this problem by FS-XFEM and XFEM is plotted in Fig. 12. The reference solution for strain energy is obtained by singular FEM with very fine mesh (1,443,082 nodes). It can be seen that FS-XFEM can produce more accurate results than XFEM with the same mesh. The stress intensity factor (SIF) is also obtained by FS-XFEM and XFEM. The SIFs with error are tabulated in Table 3. From the table, it is noticed that numerical solutions of SIFs using FS-XFEM are closer to the reference solutions than XFEM for the same mesh. This confirms that face-based smoothing technique has a strong value to integrate to XFEM.

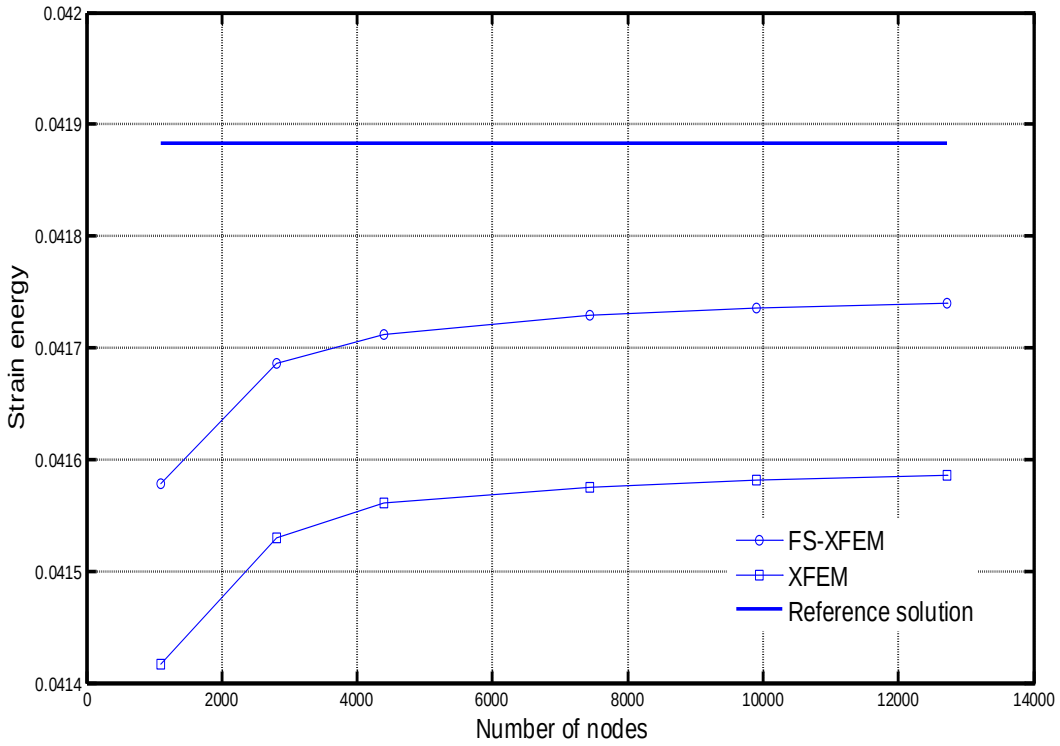

Figure 12. The variation of strain energy with number of nodes for a cylinder with a penny-shaped crack under remote tension

Table 3. $K_{\mathrm{I}}(\mathrm{MPa}\sqrt{\mathrm{mm}})$ **(with error) of FS-XFEM and XFEM for a cylinder with a penny-shaped crack under remote tension with different mesh densities**

Mesh	1352	2500	4968	6016	9306
XFEM	0.6097	0.6114	0.6118	0.612	0.6121
	(1.34%)	(1.07%)	(1%)	(0.97%)	(0.95%)
FS-XFEM	0.6121	0.6137	0.6140	0.6143	0.6144
	(0.95%)	(0.70%)	(0.65%)	(0.6%)	(0.58%)

6. Conclusion

In this work, the face-based smoothing technique is combined into extended finite element method (XFEM) to develop face-based smoothed extended finite element method (FS-XFEM) for three-dimensional fracture problems. Two numerical examples are used to test the accuracy, efficiency and convergence rate of FS-XFEM. Through the numerical results some conclusions can be drawn as follows:

1. There are no additional parameters involved in the FS-XFEM, hence, the implementation of FS-XFEM using tetrahedral element that can be generated by many commercial software is quite straightforward.
2. Due to the properly softening effects provided by the face-based smoothing technique, the proposed FS-XFEM possesses a close-to-exact stiffness of the continuous system. Hence, it can provide more accurate results than XFEM using the same tetrahedron mesh in terms of strain energy and stress intensity factors.
3. The convergence rate and computational efficiency of FS-XFEM have been improved significantly compared with XFEM. FS-XFEM also possesses some advantages compared to XFEM. For example, in the calculation of the stiffness matrix, no singular term appears in the integrand. Mapping, which increases the complexity of the calculation, is not needed.

Reference

Belytschko T. and Black T. (1999) Elastic crack growth in finite elements with minimal remeshing. Int J Numer Methods Eng 45, 601-620.

Moes N., Dolbow J. and Belytschko T. (1999) A finite element method for crack growth without remeshing. Int. J. Numer. Methods Eng 46, 131-150.

Elguedj T., Gravouil A. and Combescure A. (2006) Appropriate extended functions for XFEM simulation of plastic fracture mechanics. Comput. Methods Appl. Mech. Engrg 195, 501-515.

Bordas S., Rabczuk T. and Zi G. (2008) Three-dimensional crack initiation, propagation, branching and junction in non-linear materials by an extended meshfree method without asymptotic enrichment. Eng. Fract. Mech 75, 943-960.

Rabczuk T., Bordas S. and Zi G. (2007) A three-dimensional meshfree method for continuous multiple-crack initiation, propagation and junction in statics and dynamics. Comput. Mech 40, 473-495.

Rabczuk T., Zi G., Bordas S. and Nguyen-Xuan H. (2009) A simple and robust three-dimensional cracking-particle method without enrichment. Comput. Methods Appl. Mech. Engrg 199, 2437-2455.

Chessa J. and Belytschko T. (2003) An enriched finite element method for axisymmetric two-phase flow with surface tension. J. Comput. Phys 58, 2041-2064.

Chopp D. and Sukumar N. (2003) Fatigue crack propagation of multiple coplanar cracks with the coupled extended finite element/fast marching method. Int. J. Engrg. Sci 41, 845-869.

Merle R. and Dolbow J. (2002) Solving thermal and phase change problems with the extended finite element method. Comput. Mech 28, 339-350.

Ji, H., Chopp D. and Dolbow J. (2002) A hybrid extended finite element/level set method for modeling phase transformations. Int. J. Numer. Methods Engrg 54, 1209-1233.

Chen J.S., Wu C.T. and Yoon Y. (2001) A stabilized conforming nodal integration for Galerkin meshfree methods. Int. J. Numer. Methods Engrg 50, 435-466.

Liu G.R. and Zhang G.Y. (2009) A normed G space and weakened weak formulation of a cell-based smoothed point interpolation method. Int. J. Comput. Methods 6, 147-179.

Liu G.R. (2010) A G space theory and weakened weak (W2) form for a unified formulation of compatible and incompatible methods, part I: theory and part II: applications to solid mechanics problems. Int. J. Numer. Methods Engrg 81, 1093-1156.

Liu G.R. and Nguyen T.T. (2010) Smoothed Finite Element Method, Taylor & Francis/CRC Press: Boca Raton

Le C.V., Nguyen-Xuan H., Askes H., Bordas. S., Rabczuk T. and Nguyen-Vinh H. (2010) A cell-based smoothed finite element method for kinematic limit analysis. Int. J. Numer. Meth. Engng 83, 1651-1674.

Liu G.R., Chen L., Nguyen T.T., Zeng K.Y. and Zhang G.Y. (2010) A novel singular node-based smoothed finite element method (NS-FEM) for upper bound solutions of fracture problems. Int J Numer Meth Engng 83, 1466-1497.

Chen L., Liu G.R., Nourbakhsh N.N. and Zeng K.Y. (2010) A singular edge-based smoothed finite element method (ES-FEM) for bimaterial interface cracks. Comput Mech 45, 109-125.

Jiang Y., Tay T.E., Chen L. and Sun X.S. (2013) An edge-based smoothed XFEM for fracture in composite materials. Int. J. Fract. 179(1-2), 179-199.

Chen L., Rabczuk T., Bordas S., Liu G.R., Zeng K.Y. and Kerfriden P. (2012) Extended finite element method with edge-based strain smoothing (ESm-XFEM) for linear elastic crack growth. Comput. Methods Appl. Mech. Engrg. 209-212, 250-265.

Liu G.R., Nguyen-Thoi T. and Lam K.Y. (2008) An edge-based smoothed finite element method (ES-FEM) for static, free and forced vibration analyses of solids. J. Sound Vib. 320(4-5), 1100-1130.

Cui X.Y., Liu G.R. and Li G.Y. (2011) Bending and vibration responses of laminated composite plates using an edge-based smoothing technique. Eng. Anal. Bound Elem. 35, 818-826.

Karihaloo B.L. and Xiao Q.Z. (2003) Modelling of stationary and growing cracks in FE framework without remeshing: a state-of-the-art review. Comput. Struct. 81(3), 119-129.

Karihaloo B.L. and Xiao Q.Z. (2001) Accurate determination of the coefficients of elastic crack tip asymptotic field by a hybrid crack element with p-adaptivity. Eng. Fract. Mech 68, 1609-1630.

Xie G.Z., Zhang J.M., Huang C., Lu C.J. and Li G.Y. (2014) A direct traction boundary integral equation method for three-dimension crack problems in infinite and finite domains. Comput. Mech. 53, 575-586.

Aliabadi M.H. (1997) Boundary element formulations in fracture mechanics. Appl. Mech. Rev. 50, 83.

Cruse T.A. (1988) Boundary element analysis in computational fracture mechanics. Vol. 1 Springer Berlin.
Pan E. (1997) A general boundary element analysis of 2-D linear elastic fracture mechanics. Int. J. Fract. 88 (1), 41-59.
Nguyen-Thoi T., Liu G.R., Lam K.Y. and Zhang G.Y. (2009a) A face-based smoothed finite element method (FS-FEM) for 3D linear and geometrically non-linear solid mechanics problems using 4-node tetrahedral elements. Int. J. Numer. Meth. Engng 78, 324-353.
Nguyen-Thoi T., Liu G.R., Vu-Do H.C. and Nguyen-Xuan H. (2009b) A face-based smoothed finite element method (FS-FEM) for visco-elastoplastic analyses of 3D solids using tetrahedral mesh. Comput. Methods Appl. Mech. Engrg 198, 3479-3498
Parks D. M. (1974) A stiffness derivative finite element technique for determination of crack tip stress intensity factor. Int. J. Fracture 10, 487-502
Parks D. M. (1977) The virtual crack extension method for nonlinear material behavior. Comput. Meth. appl. Mech. Engng 12, 353-364.
Hellen T. K. (1975) On the method of virtual crack extension. Int. J. numer. Meth. Engng 9, 187-207.
Hellen T. K. (1989) Virtual crack extension methods for non-linear materials. Int. J. numer. Meth. Engng 28, 929-942.
Rybicki E. F. and Kanninen M. F. (1977) A finite element calculation of stress intensity factors by modified crack closure integral. Engng Fracture Mech. 9, 931-938
Shivakumar K. N., Tan P. W. and Newman J. C., (1988).Virtual crack closure technique for calculating stress-intensity factors for cracked three-dimensional bodies. Int. J. Fracture 36, R43-R50
Raju I. S., Shivakumar K. N. and Crews J. H. Jr. (1988).Three-dimensional elastic analysis of a composite double cantilever beam specimen. AIAA Jl 26, 1493-1498
Buchholz F. G. (1984) Improved formulae for the finite element calculation of the strain energy release rate by the modified crack closure integral method, in Accuracy Reliability and Training in FEM-Technology (Edited by J. Robinson), pp. 650-659. Robinson and Associates, Dorset
Rice J. R. (1968) A path-independent integral and the approximate analyses of strain concentration by notches and cracks. J. appl. Mech. 35, 376-386
Cherepanov G. P. (1967) Crack propagation in continuous media. J. appl. Math. Mech. 31, 503-512
Eshelby J. D. (1956) The continuum theory of lattice defects, in Solid State Physics (Edited by F. Seitz and D. Turnbull), Vol. III, pp. 79-114. Academic Press, New York.
Cherepanov G. P. (1979) Mechanics of Brittle Fracture (translated and Edited by R. W. de Wit and W. C. Cooly). McGraw-Hill, New York.
Anderson T. L. (1995) Fracture mechanics: Fundamentals and applications. Taylor & Francis Group